Correlations of projectile like fragments in heavy ion reactions at Fermi energy

Jayanti Rama Rao[1], *H. Machner*[2], *G. Buhr, M. Nolte, M. Palarczyk*
Institut für Kernphysik, Forschungszentrum Jülich, Jülich, Germany

Abstract

Correlations between pairs of projectile-like fragments, emitted by the system $^{16}O + ^{197}Au$ at the laboratory bombarding energy of 515 MeV, have been studied under two stipulated conditions: (1) at least one member of the pair is emitted at an angle less than the grazing angle for the system, (2) both the members of the pair are emitted at angles larger than the grazing angle. A surprisingly large difference, by more than an order of magnitude, is found between the correlations for the two cases. This observation could be explained on the basis of a simple semi-classical break up model. Further analysis of the variation of the charge correlation function with the difference in the nuclear charges of the correlated pair showed trends which are consistent with an "inelastic break up process", in which the projectile breaks up at the radius of contact, in such a way that, one fragment (preferably the lighter) is emitted to one side within the grazing angle, while the other orbits around the target nucleus for a while and emerges on the other side, at a negative scattering angle, much like in a deep inelastic scattering.

1 Introduction

In heavy ion reactions induced at bombarding energies below 10 MeV per nucleon the cross section for collisions is largely found in fusion and deep inelastic processes. In both channels, the interacting nuclei exhibit a large degree of coherence in the sense that very few direct third particles are emitted in the collision. Since the macroscopic velocities are small in comparison with the intrinsic speeds of nucleons, the propagation of disturbances through

[1]On leave from Benares Hindu University, Varanasi, India
[2]also at Univ. Duisburg-Essen, FB Physik, Duisburg, Germany

the whole system is rather fast. This is the reason for the manifestation of one-body mean field effects in this region.

This situation gradually changes as the bombarding energy increases. An important threshold is probably reached when the excitation energy of a nuclear system is close to its binding energy. In this case, the system largely loses its cohesion and fragmentation is more likely to set in. This limiting case is represented by an average Fermi velocity of 0.2c corresponding to a projectile energy of 20 MeV×A and an intrinsic transit time of 2.5×10^{-22}s for nuclear dimensions. Up to this point, the macroscopic features of heavy ion reactions may be characterised by a variety of equilibrating processes. They range from the fully equilibrated fusion reactions, followed by deep inelastic and quasi elastic collisions with varying degrees of equilibration, to non-equilibrating direct processes. At higher energies, when the excitation energy per nucleon increases above the Fermi kinetic energy, the quanta1 nature of nucleons is expected to become less important and the one-body mean field gives way to direct two-body collisions as the main governor of nucleonic motion.

In the scenario presented above, the intermediate energy region corresponding to the Fermi energy domain of 20 - 50 MeV per nucleon, is spoken of as "transition region" [1–4], marked by qualitative changes in the heavy ion interaction characteristics. This energy also defines the threshold for the "supersonic region", where the particle velocities exceed the velocity of sound in nuclear matter.

An important facet of interaction mechanism is the dissipation of kinetic energy of the colliding nuclei. Experimentally this is studied by the energy and angular distributions as well as the correlations between the ejectiles. However, theoretically, there seems to be a lot of confusion about this important aspect of physics in the intermediate energy region. There are two, seemingly equivalent but conceptually contradictory, viewpoints: thermodynamical and dynamical. A set of models [5–7] based on the first viewpoint envisages the occurrence of localised zones of high excitation or "hot spots", as they are called. Formation of such zones would imply that the dissipation is sufficiently effective to thermalise the collective energy in the contact zone of the colliding nuclei, whereas heat conduction is not fast enough to spread the heat over the whole nuclear system prior to particle evaporation. Present evidence for hot zones is essentially derived from light particle emission with pre-equilibrium characteristics. Their distributions are generally parameterised by Maxwellian distribution for thermal emission from hot moving sources, and, the presence of an "intermediate velocity source" in the three-source-fits serves as an identification of the hot emitting zone.

For the second set of models [8–10] based on a contradictory viewpoint,

the light particle emission is the result of a dynamical break up of the projectile. They attribute it essentially to the nuclear forces which act with different strength on different parts of the colliding projectile and thereby break the binding between its constituents. Projectile parts coming next to the target are strongly decelerated by the friction force which cuts the binding to the rest. While the "trapped" part orbits around the target for some time due to viscous drag, the broken part proceeds forward with almost the beam velocity. The whole reaction proceeds on a short time scale, without passing through a phase of (partial) thermal equilibration as a necessary intermediate step for the emission, in contradistinction to the hot spot models.

Experimentally for all ejectiles, a clear correlation is observed between their energy loss and angle of emission. But this can be explained by both the viewpoints insofar as the light particles are concerned. It has been argued that a projectile like fragment (PLF) orbiting on the target surface, shaking off light particles during and because of deceleration (and getting excited, of course) is not, conceptually and phenomenologically, distinct from a rotating hot spot.

Schwarz and collaborators [11,12] sought to clarify this situation by studying the coincident angular distributions between projectile like fragments and alpha particles. In experiments with 20 MeV×A ^{20}Ne ions bombarding ^{197}Au target, they found evidence for beam velocity alpha particles, preferentially emitted to forward angles, having correlations with strongly damped PLFs, slowed down orbiting around the target to actually negative scattering angles. Complementary to this, in an experiment with 26 MeV×A ^{32}S on ^{197}Au, fast (more than two-thirds beam velocity) PLFs proceeding at forward angles were found to be in coincidence with degraded alpha particles emitted at negative angles. Both these observations are projected to support a picture of dynamical break up of the projectile followed by the (deep inelastic) rotation of one of the fragments around the target for a while. One serious problem in resolving the ambiguity by the study of coincident angular correlations between PLFs and light particles is the sizeable and interfering contribution of such particles due to the sequential decay of the primary excited ejectiles. These events, particularly at forward angles, have to be carefully identified and eliminated to isolate and study the genuine events of direct projectile break up due to frictional forces . Experimental uncertainties in the " subtraction procedure " tend to reduce the force of the arguments. On the other hand, the coincident correlations between PLFs heavier than alpha particles are much less influenced by sequential decay. One simple way to obtain a direct signature of projectile break up vis-a-vis hot spot formation is to study the mutual correlations of all fragment pairs

emitted on either side of the beam axis and to examine the trend of correlation as a function of the opening angle between the pair of fragments. It is a well established fact [13] that the charge correlation function is modulated, not only by the extent and life time of the source emitting the particles, but also, by the dynamics of the emission process. The latter aspect is further elaborated in the next section.

2 Idea of the experiment

The inspiration for the experiment came from our previous studies on the break up of loosely bound projectiles such as deuterium and ^6Li at low bombarding energies of 25-80 MeV [14, 15]. In those studies an unmistakable evidence was found for an "inelastic break up" mode, in which the projectile breaks up into two fragments, one of which comes out from the reaction zone as a quasi elastic particle while the other fuses with the target and becomes unobservable. The energy and angular distributions of the observable spectator-like fragment could be satisfactorily explained on the basis of post DWBA formalism adapted to continuum states. Such a scenario was recently found to hold also for ^{16}O induced reactions at 25 MeV×A [16]. In view of the loss of cohesion at Fermi velocities, as pointed out earlier, the heavy ion projectile in the intermediate energy region is virtually a loosely bound entity as the composite particles at low energies. Another interesting and simplifying feature of Fermi energy regime is the expectation that a classical approach is possible for the description of heavy ion collisions and the main features of the reaction can be explained by assuming a relative motion of the nuclei along classical trajectories in the field of conservative and nonconservative (frictional) forces. As was pointed out by Strutinsky [17], the classical approach can be applied under the condition that the reduced wave length, $\lambda/2\pi = \hbar/p$, is much shorter than the range of impact parameters, δb, that contribute to the heavy ion collision. The deep inelastic reactions represent a perfect example of the classical process, since the range of angular momenta associated with these reactions, $\delta l = \delta b \times p$, is large (of the order of 100) as compared with the Planck constant $\hbar$.

In classical collisions under purely conservative fields, the classical deflection function defines the distribution of trajectories according to the impact parameter, starting from the one at the grazing angle, θ_{graz}, corresponding to the condition, $d\theta/dl = 0$, to the one at the "orbiting" angle, θ_0, corresponding to $d\theta/dl = \infty$. The latter condition occurs for an orbital angular momentum, l_{crit} where the nuclear, centrifugal and Coulomb forces balance one another ($dV/dr = 0$), the fission barrier disappears and, consequently,

the system is poised for rotation or break up. The "grazing" condition is fulfilled for l_{max} at the grazing angle, corresponding to the most peripheral collisions.

The addition of a non-conservative frictional force [18], pushes θ_0 down to negative angles, and the trajectories are deflected even to the opposite side of the grazing angle, as shown in the lower panel of Fig.1. The upper panel

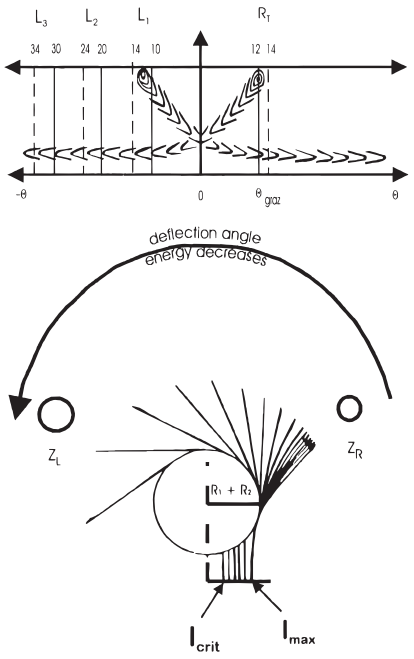

Figure 1: Lower panel: Classical trajectories of a heavy ion projectile in the mean field approximation. R_1 and R_2 are the radii of the target and projectile. Z_L and Z_R are fragments due to projectile break up caused by frictional forces at the surface (see text) . (Upper panel: Schematic contour diagram of the cross section for collision in energy-angle space. The solid and dashed vertical lines indicate the angular positions of various detectors, L_1, L_2, L_3 and R_T, for the study of fragment pair correlations (see text).

of Fig. 1 shows the distribution of cross section in energy-angle space. In the schematic contour diagram, the cross section maximum is shown by the "mountain" at the grazing angle, θ_{graz}, on one side, while its "ridge" runs all the way to (negative angles on) the other side, where the cross section is minimum. The two symmetrical branches in this diagram correspond to the possibility of scattering on either side of the target nucleus. The energy distribution shows a clear correlation with the scattering angle. For

peripheral collisions, ($l = l_{max}$), the energy losses are not very large. But with decreasing angular momentum, the trajectories are deflected towards forward (and further to negative) angles, and simultaneously, the energy losses increase.

At Fermi velocities in the transition region, the possibility of direct break up has to be superimposed on this picture. The nuclear friction provides the cutting sharp edge for the break up of the projectile moving at "supersonic" velocity. The approaching frontal part of the projectile is decelerated and cut off from the rest. Consequently, as shown in Fig. 1, one has a beam velocity projectile fragment (Z_R), preferentially scattered towards the grazing angle, while the decelerated fragment (Z_L), dragged around the target nucleus for a while, emerges (after a "deep inelastic" scattering) from the other side or may even break up into smaller fragments.

In this scenario, the study of fragment pair correlations is interesting and illuminating. For example, with two detectors on either side of the beam axis, the correlations should show a big difference, if one of the detectors is inside or outside the grazing angle. Based on this idea, the mutual correlations of all fragment pairs of the projectile are studied in this experiment, for different angular situations of the detectors as indicated in the lower panel of Fig. 1, with a view to obtain a clearer insight into the reaction mechanism at intermediate energies. This is the motivation for our work.

3 Calculation of the grazing angle

The grazing angle plays a crucial role in the model presented in the previous section. Its connection to the highest angular momentum partial wave, $l = l_{max}$ participating in a reaction and the Coulomb parameter η can be found in [19]. It would be of course the best to take this angle from experiment. Another method is to calculate the quarter-point angle, $\theta_{1/4}$, using the asymptotic values of the parameters η and wave number k, with R_{int} defined in terms of matter-half-density radii of the projectile and target. One such tabulated value [19] for the system, $^{16}O + ^{197}Au$, at $E_{lab} = 515$ MeV, was given as $\theta_{1/4} \sim 10$ degree. It depends on R_{int} the interaction radius. The value in [19] agrees nicely with the one given in [20]. However, it was pointed out [19][18] that, for strongly damped collisions, a modified value of the Coulomb parameter has to be used, as suggested by Wilczynski [18, 21], taking into account v', the relative velocity of the nuclei in the entrance channel at the interaction radius. Using Wilczynski's prescriptions [18], we have calculated the grazing angle to be about 12.5 degree for the present system. The placement angles of various detectors in the experimental set up were

chosen based on this consideration.

4 Experimental details

The experiments were carried out at the Jülich Isochronous Cyclotron. Beams of $^{16}O^{7+}$ ions at the laboratory energy of 515 MeV were transported to a scattering chamber to hit self-supporting gold targets. The beams were then dumped in a shielded Faraday cup 4m downstream. The targets were of pure gold, made by rolling, and had thicknesses of 10 mg/cm^2 for coincidence measurements and 1.5 mg/cm^2 for singles studies. For calibration purposes a deuterated polyethylene (CHD) target of thickness 12 mg/cm^2 was used. Charged particles were detected using silicon counter telescopes. The thicknesses of ΔE and E detectors were chosen according to their placement angle with respect to the beam axis. Two detector telescopes, L_1 and

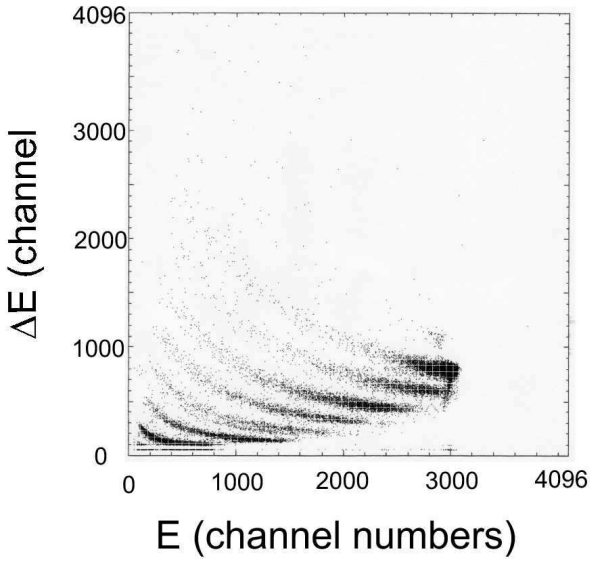

Figure 2: $\Delta E - E$ scatter plot of the telescope R_T.

R_T, placed at -l0 degrees and +12 degrees with respect to the beam had ΔE detectors of thickness 200 μm and E detectors of 5 mm each and 100 mm^2 area each. Two other telescopes, L_2 and L_3, placed at -20 degrees and -30 degrees with respect to the beam, had ΔE detectors of 50 μm and E detectors of 2 mm each, but 150 mm^2 area. All the telescopes had a veto detector of thickness 60 μm behind each of them. The right side detector, R_T, served as a trigger detector for coincidence. Its response to fragments is shown in Fig. 2. The solid angles of the telescopes, defined by apertures of Tantalum, were slightly different but they were kept the same for singles and coincidence measurements, so that they will cancel out in calculating the charge correlation function. Signals of each ΔE and E detectors as well as their sum were fed through standard electronics to analog-to-digital converters and then stored on magnetic tape in an event-mode type of recording for later off-line analysis. The procedure to balance the summation amplifiers and other details of logic circuits are reported in our previous publications [22, 23]. A typical-time spectrum for the coincidence between a pair of charged fragments, c_1 and c_2, detected at angles, $\theta_1 = 12$ degrees and $\theta_2 = -10$ degrees, is shown in Fig.3.

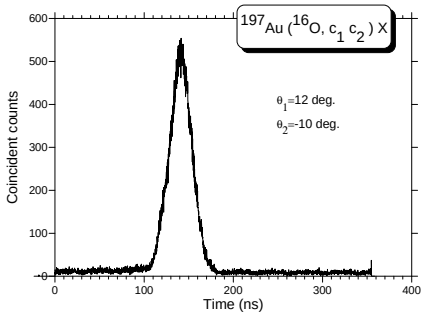

Figure 3: Time spectrum for the coincidence of two charged fragments, c_1 and c_2, emitted into the detectors at 12 degrees and -10 degrees, respectively, in the reaction $^{197}Au(^{16}O, c_1c_2)X$ at $E_{lab} = 515$ MeV.

The experiment was conducted in two parts: In the first part, the right side detector R_T was placed at +12 degrees with respect to the beam, so that it is inside the grazing angle of +12.5 degrees. The left side detectors, L_1, L_2 and L_3 were placed respectively at -l0 degrees, -20 degrees and -30 degrees, on the other side of the beam axis. These positions are indicated by the vertical solid lines in the upper panel of Fig. 1. From the viewpoint of the "mountain" at the negative grazing angle, -12.5 degrees, the detector L_1 is inside, while the others, L_2 and L_3, are outside the grazing angle. In the

second part of the experiment, the right side detector R_T was shifted to +14 degrees, so that it is completely outside the grazing angle of +12.5 degrees. At the same time the detectors, L1,L2 and L3, were shifted to -14 degrees, -24 degrees and -34 degrees, respectively, so that all of them are also outside the grazing angle. These positions are indicated by the dashed lines in the upper panel in Fig. 1.

By switching a simple AND/OR gate, the singles spectra in all the four detectors, L_1, L_2, L_3 and R_T, and, coincidence spectra between the three pairs of left and right detectors, L_1R_T,L_2R_T and L_3R_T, were recorded under identical geometrical conditions in different runs. The singles spectra of the PLFs with $Z = 2$ to $Z = 7$, were sorted out from the $\Delta E - E$ matrix of each detector using "banana" shaped gates which included all the isotopes of a given Z except for nitrogen. Since the elastic line of ^{16}O is leaking into the nitrogen band (see Fig. 2) that area has been excluded. This leads to the sharp cut off at 515 MeV in the nitrogen singles spectrum. The spikes in some of the spectra are most probably due to the limoted statistics. The coincidence spectrum of a given ordered pair of PLFs was obtained by sorting out the coincident $\Delta E - E$ matrices of the left and right detectors with appropriate banana gates corresponding to the respective PLFs. Some typical spectra are shown in Figs.3-4.

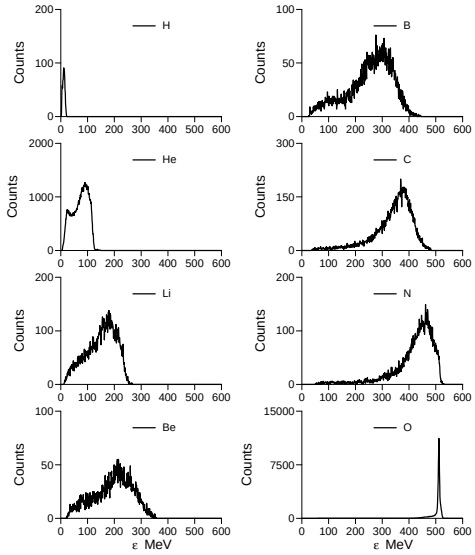

Figure 4: Singles spectra of projectile like fragments and elastically scattered oxygen at 12 degrees (lab. system).

The fragment spectra were then converted into double differential cross

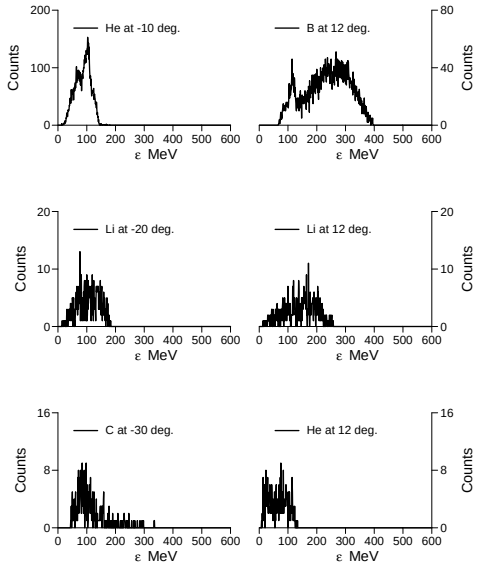

Figure 5: Typical coincidence spectra (lab. system) of fragment pairs, $He-B$, $Li-Li$ and $C-He$, detected in the left and right detectors, at the angles noted in the figure.

sections using standard formulae. Singles cross section is given by

$$\frac{d^2\sigma}{d\Omega d\epsilon} = \frac{Z_P e A_T N_s \sin\phi 10^{24}}{Q\rho L \Delta\Omega \Delta\epsilon (1-\tau/100)} \left(\frac{\text{barn}}{\text{sr MeV}}\right) \tag{1}$$

where

Z_P	Atomic number of the projectile
e	elementary charge
A_T	Atomic mass of the target (g/mol)
N_S	number of counts in the energy bin of $\Delta\epsilon$ in the singles spectrum
ϕ	Angle between target plane and beam direction
Q	Charge collected in the Faraday cup (Cb)
ρ	target thickness (g/cm^2)
L	Avogadro number (1/mol)
$\Delta\Omega$	solid angle of the detector (sr)
$\Delta\epsilon$	Width of the energy bin in the spectrum (MeV)
τ	dead time (percent)

The coincidence cross section is given by

$$\frac{d^4\sigma}{d\Omega_1 d\epsilon_1 d\Omega_2 d\epsilon_2} = \frac{Z_P e A_T N_{coi} \sin\phi 10^{24}}{Q\rho L \Delta\Omega_1 \Delta\epsilon_1 \Delta\Omega_2 \Delta\epsilon_2 (1-\tau/100)} \left(\frac{\text{barn}}{\text{sr}^2\ \text{MeV}^2}\right) \tag{2}$$

where the indices 1 and 2 refer to the PLFs detected in the left and right detectors, and N_{coi} is the corresponding number of coincidence counts for the PLF pair.

The systematic errors in the cross section measurement are: 5% error in the charge collected in the Faraday cup, 1% error in the target thickness, 5% error in dead time and 2% error in each of the solid angles (which however cancels out in the calculation of the charge correlation function). In addition, statistical errors in the singles and coincidence counting rates are taken into account for each individual case. The energy dependent Correlation function, $R(c_1, c_2)$, is usually defined in terms of the differential cross sections as

$$R(\epsilon_1, \epsilon_2) + 1 = \sigma_0 \frac{d^4\sigma(\epsilon_1\epsilon_2)}{d^2\sigma(\epsilon_1) d^2\sigma(\epsilon_2)} \tag{3}$$

where σ_0 is a constant, which involves the multiplicities of the PLFs and the total reaction cross section.

5 Results and discussion

For the purpose of studying the correlations in the present experiment, the measured double differential cross sections are integrated over the fragment energy ϵ, and redesignated as $d\sigma_{12}$for the coincidence cross section and $d\sigma_1$ and $d\sigma_2$ for the singles cross sections of the pair of fragments with atomic numbers Z_1 and Z_2. The ratio of cross sections as defined below, R_{exp}, usually termed as the experimental correlation, contains a Charge Correlation function, R_Z, given by

$$R_{exp} = \frac{R_Z + 1}{\sigma_0} = \frac{d\sigma_{12}}{d\sigma_1 d\sigma_2}. \tag{4}$$

The values of R are presented as three dimensional graphs in Figs.6-11, for various angular placements of the detectors, as a function of the atomic numbers Z_L and Z_R of the PLFs detected in the left and right detectors respectively. It can be seen from these figures that whenever the right side detector is at the angle 12 degrees, the values of R_{exp} are quite large,

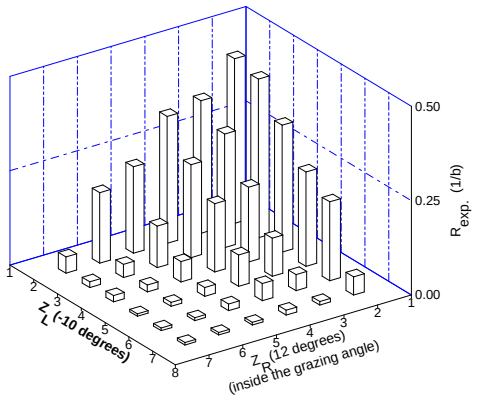

Figure 6: Three dimensional viewgraph showing the observed correlation, R_{exp}, as function of the atomic numbers, Z_L and Z_R, of the PLFs detected in the left side detector L_1 at -l0 degrees and the right side detector R_T at 12 degrees. R_T is inside the grazing angle of 12.5 degrees for the present case.

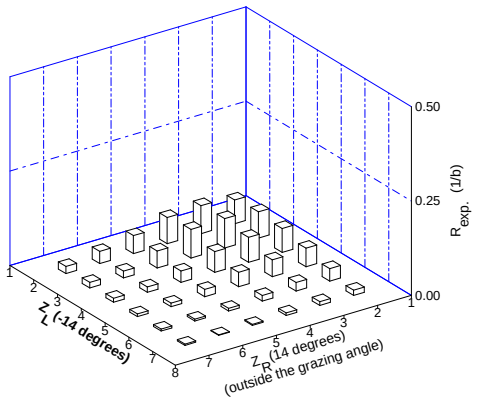

Figure 7: Same as Fig. 6, except that L_1 is at -14 degrees and R_T is at 14 degrees. R_T is outside the grazing angle of 12.5 degrees.

but when this angle is just changed to 14 degrees, the values are diminished very substantially. This observation is true for all angular positions of the left side detector from -10 degrees to -34 degrees. The sudden vanishing of the correlations for a change from 12 degrees to 14 degrees is quite significant in view of the fact that the calculated grazing angle for the present system is about 12.5 degrees as mentioned previously. At 12 degrees the right side detector is *inside* the grazing angle and for 14 degrees it is *outside* the grazing angle, even after taking into account the angular resolution of the detector,

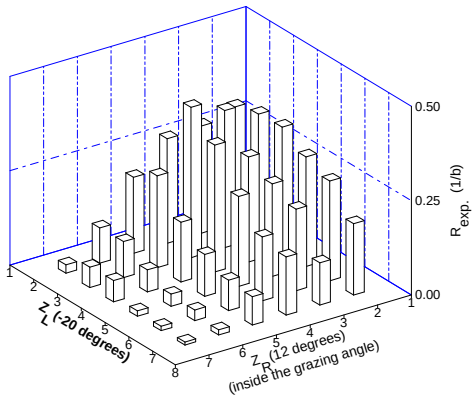

Figure 8: Same as in Fig. 6, except that L_2 is at -20 degrees. R_T is inside the grazing angle.

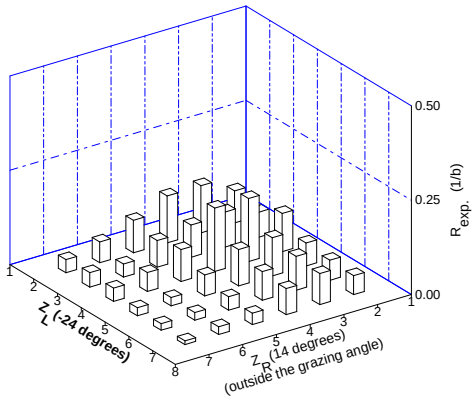

Figure 9: Same as in Fig. 7, except that L_2 is at -24 degrees. R_T is outside the grazing angle.

which is about 0.8 degrees. The big difference observed in the correlations is consistent with the expectations on the basis of the semi-classical model described in Section 2.

In order to get a quantitative idea of the correlations, we studied the variation of R_{exp} as a function of ΔZ, for an ordered pair (L,R) of PLFs, where $\Delta Z = Z_R - Z_L$ is the difference of their atomic numbers Z_L and Z_R, and they are detected in the left and right detectors respectively. Since PLFs with $Z = 2$ to 7 are detected on both sides in the present experiment, ΔZ varies from -5 to +5, for all possible pairs. The average value $< R_{exp} > = < d\sigma_{12}/d\sigma_1 d\sigma_2 >_{average}$ is calculated for each value of ΔZ, and plotted in Fig.

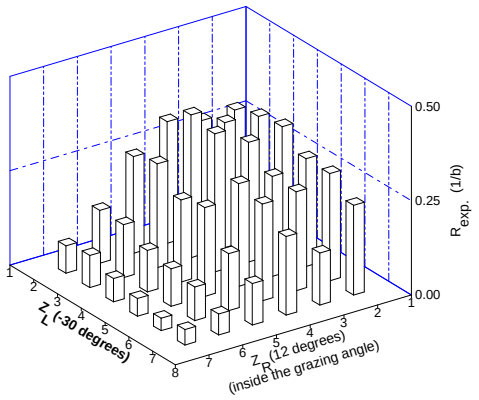

Figure 10: Same as in Fig. 6, except that L_3 is at -30 degrees. R_T is inside the grazing angle.

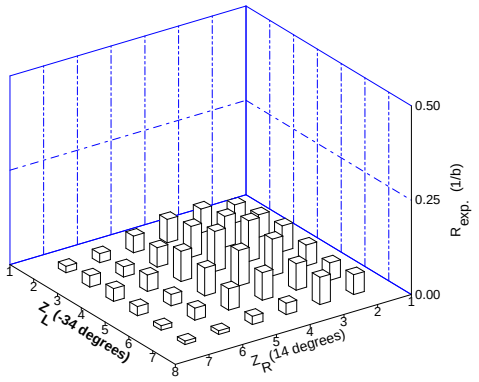

Figure 11: Same as in Fig. 7, except that L_3 is at -34 degrees. R_T is outside the grazing angle.

12, for the six angular situations of the detectors. It can be seen that the three bottom curves, (D,E,F), corresponding to the right side detector at 14 degrees (outside the grazing angle), show minimum correlation, which is taken to correspond to $R_Z = 1$, as shown by the dashed line at $< R_{exp} >= 0.057$. From this a value of 17.5 b for the normalisation constant, σ_0, is deduced.

The extracted values of the Correlation function R_Z are shown in the same 12, on the right hand side of the y-axis. It is noteworthy that the present values of R_Z for wide angle correlations of PLFs are of the same order of magnitude as those of R_q the momentum dependent Correlation function, observed in our previous study [24] of small angle correlations of alpha particles in the $^4He + ^{58}Ni$ system at 120 MeV. In the present experiment,

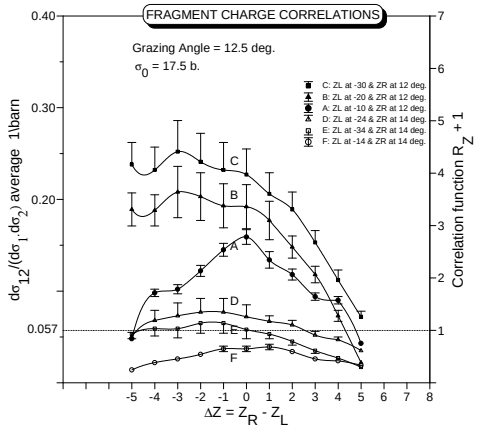

Figure 12: Trends of correlation as a function of ΔZ, the difference in the nuclear charges of the pair of projectile like fragments (see text). The curves are drawn only to guide the eye.

several interesting new features are observed in the trends of the Correlation function, which can be understood on the basis of the semi-classical model presented in Section 2:

1. The position of the right side detector, R_T, relative to the grazing angle, (θ_{graz} = 12.5 degrees), appears to act like an on/off switch, to put on and put off correlations at 12 degrees and 14 degrees respectively, irrespective of the position of the left side detectors. This behaviour can be understood by referring to Fig.1. If one imagines the PLF Z_R to be detected at the "mountain", near $+\theta_{graz}$, and the other PLF ZL to be on the left side, either at -l0 degrees, or -20 degrees, or -30 degrees, on the "ridge", then correlations always exist between them, because they originate from the interaction on the same side of the target as shown in the lower panel of Fig. 1. But, if the right side detector is at 14 degrees and the left side detectors at -14 degrees, -24 degrees and -34 degrees as shown by the dashed lines in the upper panel of Fig. 1, then, not only they are on the "opposite ridges", but more importantly, the PLFs detected by all the detectors are mainly from statistical emission from the composite system formed by lower angular momentum partial waves. Hence there is minimum or no correlation between the ejectiles.

2. The value of the Correlation function R_Z seems to increase with the negative angle of scattering of the left side PLF, as can be seen from the curves A for -10 degrees, B for -20 degrees and C for -30 degrees

in 12. This trend is again quite consistent with the model depicted in Fig. 1 and discussed in Section 2. It can be explained as follows: With increasing relative angle, the background contribution from the uncorrelated statistical emission decreases very fast, thus leaving only the real correlated events to dominate.

3. It is curious that, while the curve A in 12 corresponding to Z_L at -10 degrees and Z_R at 12 degrees is symmetrical about $\Delta Z = 0$, the curves B and C corresponding to Z_L at -20 degrees and -30 degrees, respectively, are asymmetric. Further, the curves B and C are rather constant for negative Δ_Z, that is, when Z_L detected on the left side is larger than Z_R detected on the right side. This indication lends support to our idea of inelastic break up, in which a small fragment of the projectile breaks away, without much energy loss, preferentially towards the grazing angle, while the rest of the projectile undergoes a large dissipation of energy in a kind of deep inelastic scattering around the target nucleus. This is a new reaction mode, which is clearly distinct from the "free" or elastic break up (with no energy dissipation) observed at higher energies, as well as from the so called "incomplete fusion" observed at lower energies.

In all cases shown in Figs 6 to 11 one can clearly see events in which sum of the atomic numbers of two projectile-like fragments is larger than the charge of the oxygen projectile. It is very likely that these are the events where ^{16}O projectile breaks into two parts - one which continue to move with almost the projectile velocity, and the second, which while orbiting around the target nucleus is "receiving" some matter from the target and is emerging with higher nuclear charge than originally having. The longer is the orbiting time (i.e. larger the absolute value of θ_2), probability for this kind of events is increasing which is also seen when comparing e.g. Figs. 6, 8 and 10. This could in part also explain a difference in shapes of curves A, B and C seen in Fig. 12.

A series of studies of the present system $^{16}O +^{197} Au$ at bombarding energies comparable to the nucleonic Fermi energy have bee performed in the past. They mostly concentrated on fragmentation into α particles or α cluster nuclei [8, 25, 26]. This seems to be a to limiting view. From the two dimensional charge correlation functions it is evident that for instance correlations with lithium are as abundant as with helium. Pouliot et al. [27] measured mainly light-light and heavy-light coincidences including channels up to five light fragments. Their main interest are those channels where the sum of all fragments is the projectile. The present work is complementary

to these studies. Previous studies found strong correlation between nucleons and projectile fragments [28], with the projectile emission angle within the grazing angle. On the whole, the presently observed fragment–fragment correlations in the highly asymmetric $^{16}O + ^{197}Au$ system, indicate the persistence of the binary reaction dynamics, with slight modifications, at the onset of intermediate energy regime. More exclusive and detailed studies of fragment–fragment correlations are needed for a clear understanding of the reaction mechanism in the intermediate energy region.

6 Summary and conclusions

In summary, the trends of fragment–fragment correlations observed in the present experiment support the idea of an "inelastic break up process", in which the projectile breaks up at the radius of contact, in such a way that, one fragment (preferably the lighter) is emitted to one side within the grazing angle, while the second fragment orbits around the target nucleus for a while and emerges on the other side, at a negative scattering angle, much like in a deep inelastic scattering. Such a model nicely fits into the evolutionary nature of the transition region, and, into the sequence of gradually changing interaction characteristics from one-body mean field effects to two-body collision dynamics.

Acknowledgement

The authors wish to thank the Cyclotron staff of JULIC for their nice cooperation. One of the authors (JRR) is grateful to the Internationales Büro, BMFT, for supporting his stay in Jülich.

References

[1] E. Suraud, Ch. Gregoire, B. Tamain, Progr. Part. Nucl. Phys. **23**, 357 (1989).

[2] D.H.E. Gross, Rep. Progr. Phys. **53**, 605(1990).

[3] L.G. Moretto, G.J. Wozniak, Annu. Rev. Nucl. Part. Sci. **43**, 379 (1993).

[4] H. Fuchs, K. Moehring, Rep. Progr. Phys. **57**, 231 (1994).

[5] J.P. Bondorf, R. Donangelo, I.N. Mishustin, H. Schulz, Nucl. Phys. **A 444**, 460 (1985).

[6] S.E. Koonin, J. Randrup, Nucl. Phys. **A474**, 173 (1987).

[7] W.A. Friedman, Phys. Rev. **C 42**, 667 (1990).

[8] K. Moehring, T. Srokowski, D.H.E. Gross, Nucl. Phys. **A 533**, 333 (1991).

[9] A. Bonasera, A., M. Di Toro, C. Gregoire, Nucl. Phys. **A 463**, 653 (1987).

[10] G. Royer, Y. Raffray, A. Oubahadou, B. Remaud, Nucl. Phys. **A 466**, 139 (1987).

[11] C. Schwarz, H. Fuchs, H. Homeyer, K. Moehring, A. Siwek, A. Sourell, W. Terlau, A. Budzanowski, Phys. Lett. **B 279**, 223 (1992).

[12] W. Terlau, M. Buergel, A. Budzanowski, H. Fuchs, H. Homeyer, G. Roeschert, J. Uckert, R. Vogel, Z. Phys. A - Atoms and Nuclei **330**, 303 (1988).

[13] D.H. Boal, C.K. Gelbke, B.K. Jennings, Rev. Mod. Phys. **62**, 553 (1990).

[14] J. Pampus, J. Bisplinghoff, J. Ernst, T. Mayer-Kuckuk, J. Rama Rao, G. Baur, F. Roesel, D. Trautmann, Nucl. Phys. **A 311**, 141 (1978).

[15] U. Bechstedt, H. Machner, G. Baur, G., R. Shyam, C. Alderliesten, O. Bousshid, A. Djaloeis, P. Jahn, C. Mayer-Boericke, F. Roesel, D. Trautmann, Nucl. Phys. **A 343**, 221 (1980).

[16] E. Gadioli *et al.*, Nucl. Phys. **A 708**, 391 (2003).

[17] V.M. Strutinsky, ZETP (USSR) **46**, 2078 (1964).

[18] J. Wilczynski, Nucl. Phys. **A 216**, 386 (1973).

[19] W. W. Wilcke, J.R. Birkelund, H.J. Wollersheim, A.D. Hoover, J.R. Huizenga, W.U. Schroeder, L.E. Tubbs, Atom. Nucl. Data Tables **25**, 389 (1980).

[20] P. Roussel et al., Nucl. Phys. **A 477**,345 (1988).

[21] J. Galin, J. Phys. **G5**, 83 (1976).

[22] H. Machner, D. Protic, G. Riepe, H.G. Bohlen, H. Fuchs, Phys. Rev. **C 31**, 443 (1985).

[23] G. Buhr, H. Machner, M. Nolte, M. Palarczyk, J. Rama Rao, Phys. Rev. **C 45**, 705 (1992).

[24] H. Machner, M. Palarczyk, H.W. Wilschut, M. Nolte, E.E. Koldenhof, Phys. Lett. **B 280**, 16 (1992).

[25] B. A. Harmon et al., Phys. Lett. **B 235**, 234 (1990).

[26] D. O'Kelly et al., Phys. Lett. **B 393**, 301 (1997).

[27] J. Pouliot et al., Phys. Rev. **C 43**, 735 (1991).

[28] P. Roussel *et al.*, J. Phys. G. **26**, 1641 (2000).